Journal of the Physical Society of Japan
Vol. 69, No. 9, September, 2000, pp. 3107-3114

Nonlocal Screening Effect in Cu $4p_\sigma$-$1s$ Resonant X-ray Emission Spectra in Nd_2CuO_4

Tsuyoshi IDÉ* and Akio KOTANI[1,**]

IBM Research, Tokyo Research Laboratory, 1623-14 Shimotsuruma, Yamato, Kanagawa 242-8502
[1]*Institute for Solid State Physics, University of Tokyo, Kashiwanoha 5-1-5, Kashiwa, Chiba 277-8581*

(Received May 25, 2000)

We theoretically study polarization and momentum-transfer dependence in Cu $4p_\sigma$-$1s$ resonant X-ray emission spectra (RXES) of Nd_2CuO_4 with exact diagonalization techniques, developing our previous report [T. Idé and A. Kotani, J. Phys. Soc. Jpn. **68** (1999) 3100]. We explain the experimental polarization and angular dependence of a charge-transfer excitation about 5.7 eV above the ground state. Comparing results calculated with single- and multi-Cu models, we confirm the essential contribution of the nonlocal screening effect in Cu $4p_\sigma$-$1s$ RXES, together with the configuration dependence of d-p hybridization. We predict considerable dependence of a CT excitation at about 2 eV on momentum transfer along the CuO_2 planes, and the 5.7 eV excitation has less dependence.

KEYWORDS: resonat X-ray emission, insulating cuprates, incident energy dependence, nonlocal screening effect, configuration dependence, Lanczos method

§1. Introduction

Resonant X-ray emission spectroscopy (RXES) occupies a unique position in material science in that it offers rich information on electronic structures in terms of both local and translational selection rules. With well-polarized X-rays created by synchrotron light sources, several groups have reported angular and polarization dependence of RXES in these days,[1-5] and derived significant information on electronic structures.

Most of theoretical studies on polarization dependence of RXES in d and f electron systems within the framework of the second-order optical process have been based on impurity Anderson models so far. The applicability of impurity Anderson models to angle or polarization resolved RXES is mathematically understood from the explicit formula of the scattering cross section, where the scattering amplitude of the whole crystal is expressed as Fourier transformation of the local scattering amplitude of angular and polarization dependence (see eq. (2.4)). As far as the Cu $4p$-$1s$ RXES of Nd_2CuO_4 is concerned, however, it is also apparent that the impurity limit disregards, first, the nonlocal screening effect due to the Zhang-Rice singlet formation, and second, the momentum transfer ($\boldsymbol{q}$) dependence of RXES.

In this paper, we discuss the polarization dependence in Cu $4p$-$1s$ RXES of Nd_2CuO_4, extending our previous paper.[6] While definite polarization dependence of Cu K-XAS in this material has been already reported by a number of authors,[7-9] little has been known about polarization dependence of RXES. Since a $1s$ orbital has no orbital degeneracy, theoretical analysis on polarization dependence is much simpler than that of, *e.g.*, $3d$-$2p$ transition.[10] Furthermore, the absence of apex oxygen in Nd_2CuO_4 and no overlap between $4p_\pi$ and $4p_\sigma$ absorption edges make the situation clearer. Recently, the polarization dependence of Cu $4p$-$1s$ RXES of Nd_2CuO_4 has been experimentally measured by Hill *et al.*[11] and Hämäläinen *et al.*.[12] Thus comparison with experimental data offers us a plain confirmation on the theoretical framework of RXES.

In our previous study on Cu $4p_\pi$-$1s$ RXES of Nd_2CuO_4,[6] we have proposed the nonlocal screening mechanism for the absence of resonance enhancement when the main Cu K-absorption peak is targeted by an incident X-ray. It was the first quantitative study that demonstrates the essential role of the nonlocal screening effect[13-15] in RXES. Figure 1 summarizes the physical picture. When the incident X-ray with energy Ω is targeted at the main peak of XAS, the strong $1s$-$3d$ Coulomb repulsive interaction pushes out a $3d$ hole to the neighboring plaquette to form a Zhang-Rice (ZR) singlet. In other words, a $3d$ hole gets to move over the CuO_2 plane due to "potential doping". Since this intermediate state is an "inter-plaquette" excitation, the overlap with an "intra-plaquette" excitation is small, and that with an inter-plaquette excitation is large. The Ω dependence of RXES spectra is mainly ruled by the spatial extent of charge-transfer excitations.

In this explanation, we do not use detailed characters on the spatial direction of $4p$ orbitals. Hence when the experimental data with differently polarized photon can be successfully interpreted with the same theory, an ideal justification of the theory is found. At the same time, it is interesting to investigate whether the anisotropy in $4p$ orbitals affects the screening process in the valence electronic state. We will show that the polarization dependence in RXES can be clearly understood in terms of the framework of the second-order optical process. We

* E-mail: goodidea@jp.ibm.com
** E-mail: kotani@issp.u-tokyo.ac.jp

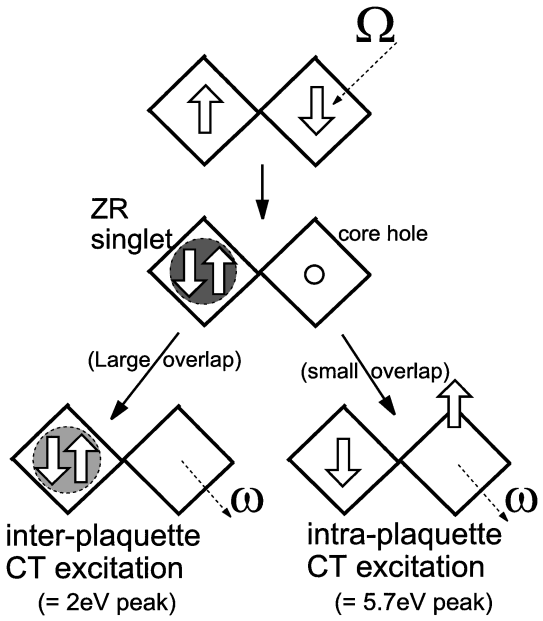

Fig. 1. Physical picture of nonlocal effect of Cu 1s-4p-1s RXES when the incident photon energy Ω is tuned at the main peak of XAS.

will also show that Cu $4p_\sigma$-1s spectra essentially follow $4p_\pi$-1s spectra discussed in the previous result.

The other point that the impurity limit disregards is the $\boldsymbol{q}$-dependence of RXES. Momentum resolved RXES with hard X-rays is a complement to angle-resolved PES to examine the entire Brillouin zone. Recently, the $\boldsymbol{q}$-dependence of RXES is measured for Mott-Hubbard systems[16,17] and insulating cuprates.[18] Despite of their significance, there have been few theoretical studies on the $\boldsymbol{q}$-dependence so far. Very recently, Tsutsui, Tohyama and Maekawa reported a numerical calculation on the $\boldsymbol{q}$-dependence of Cu 4p-1s RXES for the fist time.[19] Based on an effective 4×4 Hubbard model, they discussed the energy dispersion of the CuO_2 planes of insulating cuprates. Within one-dimensional (1D) systems, we will show a model calculation on the $\boldsymbol{q}$-dependence of Cu 4p-1s RXES of cuprates, and derive valuable information in the context of local and nonlocal excitations in Nd_2CuO_4.

The layout of this paper is as follows. In the next section, the formulae for angular dependent transition operators are given. In §3, we explain experimental polarization dependence with those formulae. In §4, the role of the nonlocal screening effect is briefly described. In §5, we discuss intra- and inter-plaquette natures of CT excitations from a viewpoint of the $\boldsymbol{q}$-dependence of RXES. In the final section, a brief summary is given.

§2. Formulation

2.1 Hamiltonian

We use a periodic Anderson model including Cu 1s, $3d(x^2-y^2)$ and 4p, as well as σ-bonding O 2p orbitals. The total Hamiltonian is given by

$$H = H_{dp} + H_{\rm core} + H_{4p3d} + H_{4p\sigma}.$$

We define creation operators at a site $\boldsymbol{R}$ for Cu 1s, 3d, $4p_\zeta$ ($\zeta = x,y,z$) and O 2p as $S^\dagger_{\boldsymbol{R}}$, $d^\dagger_{\sigma\boldsymbol{R}}$, $Q^\dagger_{\boldsymbol{R}\zeta}$ and $p^\dagger_{\sigma\boldsymbol{R}}$, respectively. The spin quantum number σ ($=\uparrow$ or $\downarrow$) is neglected for 1s and 4p orbitals. H_{dp} is the standard d-p Hamiltonian:

$$\begin{aligned} H_{dp} = &-\Delta \sum_{\boldsymbol{R},\sigma} d^\dagger_{\sigma\boldsymbol{R}} d_{\sigma\boldsymbol{R}} + \sum_{\langle \boldsymbol{r},\boldsymbol{r}'\rangle,\sigma} T_{pp}\left(p^\dagger_{\sigma\boldsymbol{r}} p_{\sigma\boldsymbol{r}'} + \text{H.c.}\right) \\ &+ \sum_{\langle \boldsymbol{R},\boldsymbol{r}\rangle,\sigma} T_{pd}\left(d^\dagger_{\sigma\boldsymbol{R}} p_{\sigma\boldsymbol{r}} + \text{H.c.}\right) \\ &+ U_{dd} \sum_{\boldsymbol{R}} d^\dagger_{\uparrow\boldsymbol{R}} d_{\uparrow\boldsymbol{R}} d^\dagger_{\downarrow\boldsymbol{R}} d_{\downarrow\boldsymbol{R}} \\ &+ U_{pp} \sum_{\boldsymbol{r}} p^\dagger_{\uparrow\boldsymbol{r}} p_{\uparrow\boldsymbol{r}} p^\dagger_{\downarrow\boldsymbol{r}} p_{\downarrow\boldsymbol{r}}. \end{aligned}$$

$H_{\rm core}$ involves 1s-3d and 1s-4p correlation,

$$\begin{aligned} H_{\rm core} = &\varepsilon_{1s} \sum_{\boldsymbol{R}} S^\dagger_{\boldsymbol{R}} S_{\boldsymbol{R}} \\ &+ U_{dc} \sum_{\boldsymbol{R}} \left(\sum_\sigma d^\dagger_{\sigma\boldsymbol{R}} d_{\sigma\boldsymbol{R}}\right) S_{\boldsymbol{R}} S^\dagger_{\boldsymbol{R}} \\ &- \sum_{\boldsymbol{R}} \left(\sum_\zeta U_{4pc} Q^\dagger_{\zeta\boldsymbol{R}} Q_{\zeta\boldsymbol{R}}\right) S_{\boldsymbol{R}} S^\dagger_{\boldsymbol{R}}. \end{aligned}$$

The Cu 3d-4p correlation is also explicitly considered,

$$H_{4p3d} = -\sum_{\boldsymbol{R}} \left(\sum_\zeta U_{4p3d}(\zeta) Q^\dagger_{\zeta\boldsymbol{R}} Q_{\zeta\boldsymbol{R}} \sum_\sigma d^\dagger_{\sigma\boldsymbol{R}} d_{\sigma\boldsymbol{R}}\right).$$

Finally, the one-electron part $H_{4p\sigma}$ is defined by

$$\begin{aligned} H_{4p\sigma} = &\varepsilon_{4p\sigma} \sum_{\boldsymbol{R}} \sum_{\eta=x,y} Q^\dagger_{\eta\boldsymbol{R}} Q_{\eta\boldsymbol{R}} \\ &+ t_1 \sum_{\boldsymbol{R}} \left(Q^\dagger_{x\boldsymbol{R}} Q_{x,\boldsymbol{R}+a\hat{x}} + Q^\dagger_{y\boldsymbol{R}} Q_{y,\boldsymbol{R}+a\hat{y}} + \text{H.c.}\right) \\ &+ t_2 \sum_{\boldsymbol{R}} \left(Q^\dagger_{x\boldsymbol{R}} Q_{x,\boldsymbol{R}+a\hat{y}} + Q^\dagger_{y\boldsymbol{R}} Q_{y,\boldsymbol{R}+a\hat{x}} + \text{H.c.}\right), \end{aligned}$$

where $\hat{x}$ and $\hat{y}$ are two unit vectors along Cu-O direction in the CuO_2 plane. a is the Cu-O distance.

Calculated results are obtained mainly with a Cu_5O_{16} cluster (Fig. 2(a)), where we adopt open boundary condition. Except for $t_1 = 0.24$ and $t_2 = -0.8$, and $U_{4p3d} = 3.3\,$eV, all parameters are the same as those of the previous study:[6] $\Delta = 2.5$, $|T_{pd}| = 1.21$, $|T_{pp}| = 0.55$, $U_{dd} = 2U_{pp} = 8.8$, $U_{dc} = 7.5$, $U_{4p3d} = 3.0$ and $U_{4pc} = 4.0\,$eV. For the 4p-4p transfer energy parameters t_1 and t_2, we consider a first principle band calculation.[20] The difference between $U_{4p3d}(\sigma)$ and $U_{4p3d}(\pi)$ due to multipole contribution of the Slater integrals is estimated as $0.34\,$eV with Cowan's numerical program[21] together with the empirical reduction factor 0.85, from which we take the value 3.3 for $U_{4p3d}(\sigma)$.

In addition, we define an impurity Anderson model in Fig. 2(b). In order to keep the main-satellite energy separation of XAS to be the same as that of the large cluster model, a different parameter $\Delta = 1.5\,$eV is used for this model.[13]

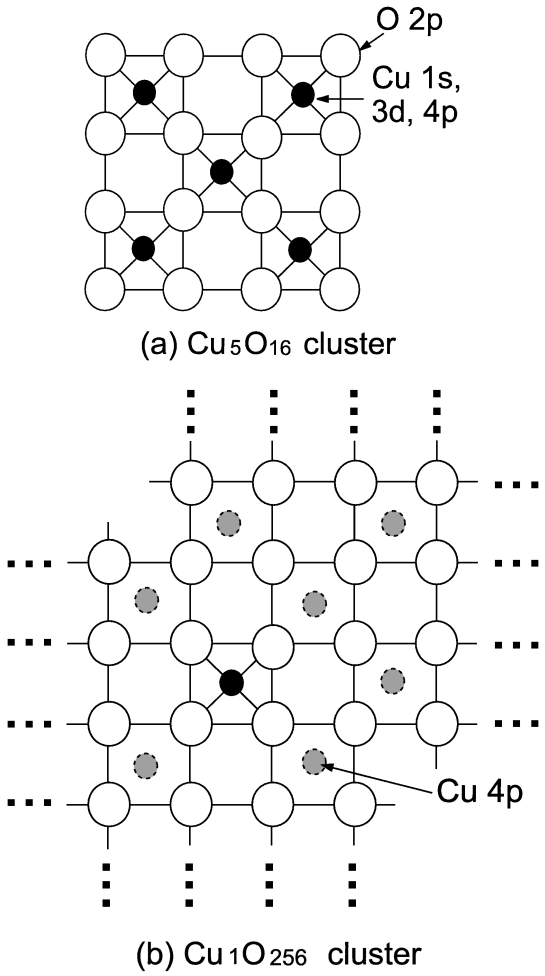

Fig. 2. The Cu_5O_{16} and the Cu_1O_{256} (impurity Anderson) models. The closed circles represent Cu $\{1s, 3d_{x^2-y^2}, 4p\}$ orbitals, and the open circles represent O $2p$ orbitals σ-bonding to the neighboring Cu $3d_{x^2-y^2}$ orbitals. Note that the full Cu $4p$-$4p$ network is taken into account in the impurity Anderson model, although all Cu $1s$ and $3d$ orbitals except for the central ones are neglected.

2.2 Angular-dependent transition operators

For the $1s$ excitation, it is appropriate for $4p$ operators to be expressed under the Cartesian coordinates, $(4p_x, 4p_y, 4p_z)$. The definition of the coordinates, whose origin is fixed to a Cu site, is described in Fig. 3. We set unit vectors along the x, y and z axes to be $\hat{e}_x$, $\hat{e}_y$ and $\hat{e}_z$. In the atomic dipole approximation, we immediately have the $1s$-$4p$ absorption operator as

$$T^{\rm a}_{\boldsymbol{\epsilon}}(\boldsymbol{R}) = \boldsymbol{\epsilon} \cdot \sum_{\zeta=x,y,z} \hat{e}_\zeta Q^\dagger_{\zeta\boldsymbol{R}} S_{\boldsymbol{R}},$$

where we dropped a trivial prefactor.

Let us define another set of unit vectors, $\hat{x}_1$ and $\hat{y}_1$, which are parallel and perpendicular to the scattering plane, respectively. Both are perpendicular to the incident wave vector $\boldsymbol{q}_1$. Experimentally, it is convenient to express the polarization vector in terms of these unit vectors,

$$\boldsymbol{\epsilon} = \sum_{\alpha=\hat{x}_1,\hat{y}_1} \epsilon_\alpha \hat{\alpha}.$$

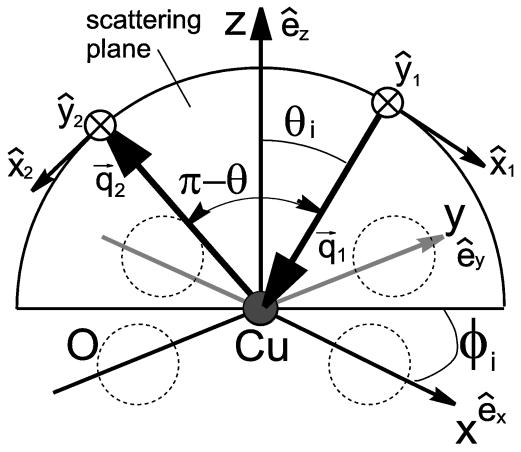

Fig. 3. Geometrical configuration of RXES. The semicircle represents the scattering plane. The solid and open circles are Cu and O atoms, respectively. x and y axes are taken along two Cu-O directions. ϕ_i and θ_i designate the direction of the wave vector of the incident photon, $\boldsymbol{q}_1$. $\boldsymbol{q}_2$ is the wave vector of the emitted photon with a scattering angle θ. The polarization vector of the incident photon is described in terms of unit vectors $\hat{x}_1$ and $\hat{y}_1$. The former is parallel to the scattering plane, whereas the latter (not shown in the figure) is perpendicular to the scattering plane. These agree with each of the unit vectors of the x and y axes, respectively, in the limit ϕ_i, $\theta_i \to 0$. The polarization vector of the emitted photon is described with $\hat{x}_2$ and $\hat{y}_2$, which agree with $\hat{x}_1$ and $\hat{y}_1$, respectively, in the limit ϕ_i, θ_i and $\theta \to 0$.

Hence we obtain

$$T^{\rm a}_{\boldsymbol{\epsilon}}(\boldsymbol{R}) = \sum_{\zeta,\alpha} \epsilon_\alpha (\hat{\alpha} \cdot \hat{e}_\zeta) Q^\dagger_{\zeta\boldsymbol{R}} S_{\boldsymbol{R}}. \tag{2.1}$$

On the analogy of $T^{\rm a}_{\boldsymbol{\epsilon}}(\boldsymbol{R})$, the $4p$-$1s$ X-ray emission operator is given by

$$T^{\rm e}_{\boldsymbol{\epsilon}'}(\boldsymbol{R}) = \sum_\zeta \sum_{\beta=\hat{x}_2,\hat{y}_2} \epsilon'_\beta (\hat{\beta} \cdot \hat{e}_\zeta) S^\dagger_{\boldsymbol{R}} Q_{\zeta\boldsymbol{R}}, \tag{2.2}$$

where $\hat{x}_2$ and $\hat{y}_2$ are unit vectors parallel and perpendicular to the scattering plane, respectively, defined for the emitted wave vector $\boldsymbol{q}_2$ (see Fig. 3). Hence we have the transition operator of RXES at $\boldsymbol{R}$,

$$T_{\boldsymbol{\epsilon}'\boldsymbol{\epsilon}}(\boldsymbol{R};\Omega) = \sum_{\alpha,\beta,\zeta} \epsilon'_\beta D^\zeta_{\hat{\beta}\hat{\alpha}}(\theta,\theta_i,\phi_i)\epsilon_\alpha \times S^\dagger_{\boldsymbol{R}} Q_{\zeta\boldsymbol{R}} G_0(\Omega) Q^\dagger_{\zeta\boldsymbol{R}} S_{\boldsymbol{R}}, \tag{2.3}$$

where $D^\zeta_{\hat{\beta}\hat{\alpha}}(\theta,\theta_i,\phi_i) \equiv (\hat{\beta} \cdot \hat{e}_\zeta)(\hat{e}_\zeta \cdot \hat{\alpha})$ is tabulated in table I. $G_0(\Omega)$ is the resolvent operator defined by $(\Omega + E_g - H + {\rm i}\Gamma)^{-1}$. We take $\Gamma = 0.8\,{\rm eV}$. Eventually, the overall operator of RXES is given by

$$T_{\boldsymbol{\epsilon}'\boldsymbol{\epsilon}}(\Omega) = \sum_{\boldsymbol{R}} {\rm e}^{{\rm i}\boldsymbol{q}\cdot\boldsymbol{R}} T_{\boldsymbol{\epsilon}'\boldsymbol{\epsilon}}(\boldsymbol{R};\Omega), \tag{2.4}$$

where $\boldsymbol{q} = \boldsymbol{q}_2 - \boldsymbol{q}_1$ is the momentum-transfer of the X-ray.

§3. Polarization Dependence

3.1 Experimental data

Experimental data were measured by Hill *et al.*[11] and Hämäläinen *et al.*[12] for a single crystal of Nd_2CuO_4 un-

Table I. Angular dependent function $D^{\zeta}_{\hat{\beta}\hat{\alpha}}(\theta, \theta_i, \phi_i)$.

$(\hat{\beta}, \hat{\alpha})$	x	y	z
$(\hat{x_2}, \hat{x_1})$	$\cos(\theta_i+\theta)\cos\theta_i\cos^2\phi_i$	$\cos(\theta_i+\theta)\cos\theta_i\sin^2\phi_i$	$\sin(\theta_i+\theta)\sin\theta_i$
$(\hat{y_2}, \hat{x_1})$	$-\cos\theta_i\sin\phi_i\cos\phi_i$	$\cos\theta_i\sin\phi_i\cos\phi_i$	0
$(\hat{x_2}, \hat{y_1})$	$-\cos(\theta_i+\theta)\cos\phi_i\sin\phi_i$	$\cos(\theta_i+\theta)\cos\phi_i\sin\phi_i$	0
$(\hat{y_2}, \hat{y_1})$	$\sin^2\phi_i$	$\cos^2\phi_i$	0

der two geometries depicted in Fig. 4. In the geometry (a), both polarization vectors, $\boldsymbol{\epsilon}$ and $\boldsymbol{\epsilon}'$, are parallel to the scattering plane, and they take 30° to the z-axis (so-called c-axis). In the geometry (b), both polarization vectors are perpendicular to the scattering plane, being parallel to the ab-plane. Note that the momentum transfer vector is common to both geometries.

The upper panel of Fig. 5 shows Cu K-XAS spectra for both geometries.[12] We observe four distinct bumps from A to D for the geometry (a), which is denoted by "$\boldsymbol{\epsilon} \sim \|c$" in the figure, whereas only two structures C and D are observed for the geometry (b), which is denoted by "$\boldsymbol{\epsilon}\|ab$". The *first* question to be answered is this polarization dependence.

Analogous to Cu $4p_\pi$-$1s$ RXES,[6,11] where the geometry (a) is adopted, a charge-transfer (CT) excitation is observed at about 5.7 eV energy loss also under the geometry (b). The Ω-dependence of the 5.7 eV intensity is plotted in the lower panel of Fig. 5 for both geometries. The experimental Ω-scan represented with the open circles is just the same data as in refs. 11 and 6. As seen in the figure, strong resonance enhancement is observed only when Ω passes by the absorption peak B in the case of the geometry (a). On the other hand, strong enhancement occurs only when Ω passes by the absorption peak D in the case of the geometry (b). To confirm this, RXES spectra under the two geometries with $\Omega = \Omega_{\rm B} \equiv 8990$ eV (peak B) and $\Omega_{\rm D} \equiv 8999.5$ eV (peak D) are shown in the lower and upper panels in Fig. 6, respectively. We see that the inelastic peak is observed at about 5.7 eV in both geometries. However, no enhancement occurs in the geometry (b) when Ω is tuned at B (lower panel). This is the *second* question. Conversely, no enhancement occurs in the geometry (a) when Ω is tuned at D (upper panel). This is the *third* question. Moreover, the maximum intensity of the 5.7 eV peak is considerably different in both cases. This is the *fourth* question.

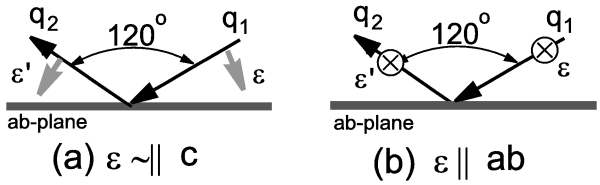

Fig. 4. The experimental geometries. (a) Polarization vectors of the incident and emitted photons are parallel to the scattering plane ("$\boldsymbol{\epsilon} \sim \|c$"). (b) Polarization vectors of the incident and emitted photons are perpendicular to the scattering plane ("$\boldsymbol{\epsilon}\|ab$"). For both (a) and (b), the scattering angle is $\theta = 60°$, and the momentum transfer vector is perpendicular to the CuO_2 plane (so-called ab-plane).

3.2 *Theoretical explanation*

For theoretical description, we put an assumption, as the lowest nontrivial approximation, that difference between σ and π in U_{4pd}, U_{4pc} and $4p$-$4p$ transfers do not substantially change the valence states in the intermediate state. Let us first consider the angular dependence of K-XAS. We easily see from eq. (2.1) that only $4p_\sigma$ absorption, i.e. excitation to a $4p_x$ or a $4p_y$ orbital, occurs when $\boldsymbol{\epsilon} = \hat{y}_1$ (the geometry (b)). This is the reason of the double-peak structure in the XAS spectrum in Fig. 5

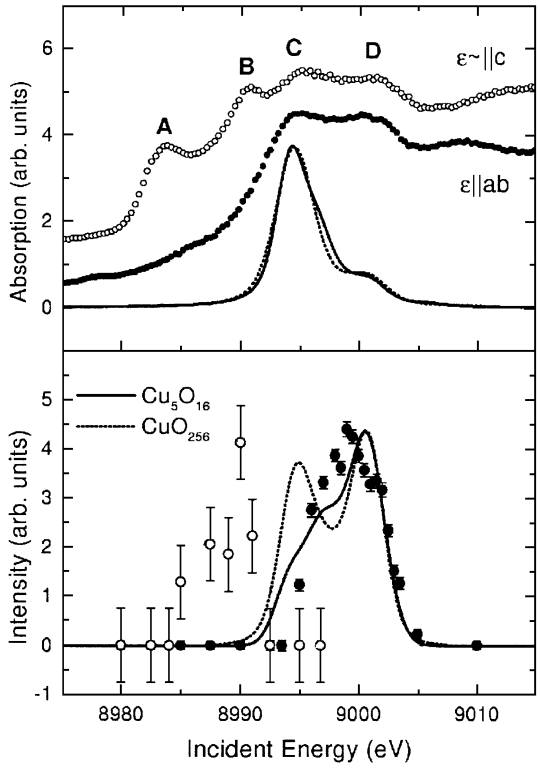

Fig. 5. *Upper panel*: Cu K-XAS of Nd_2CuO_4.[12] The open and closed circles represent experimental data under the geometries (a) and (b), respectively. The solid and dotted curves represent calculated Cu $1s \to 4p_\sigma$ absorption spectra under the geometry (b) with the multi-Cu and single-Cu models, respectively. Both curves are convoluted with Lorentzian $\Gamma_L = 0.8$ eV (HWHM) to consider lifetime of a $1s$ hole, and further convoluted with Gaussian $\Gamma_G = 0.8$ eV (HWHM) for the multi-Cu model, and with $\Gamma_G = 1.2$ eV (HWHM) for the single-Cu model to reproduce the experimental line width. *Lower panel*: the Ω-dependence of the 5.7 eV intensity.[12] The definition of the open and closed circles is the same as the upper panel. The solid and dotted curves represent the Ω-dependence of intensity of the 5.7 eV peak in Cu $4p_\sigma$-$1s$ RXES calculated under the geometry (b) with the multi-Cu and single-Cu models, respectively. Both curves are convoluted with $\Gamma_G = 1.10$ eV (HWHM) for the incident X-ray and with $\Gamma_G = 1.15$ eV (HWHM) for the emitted X-ray.

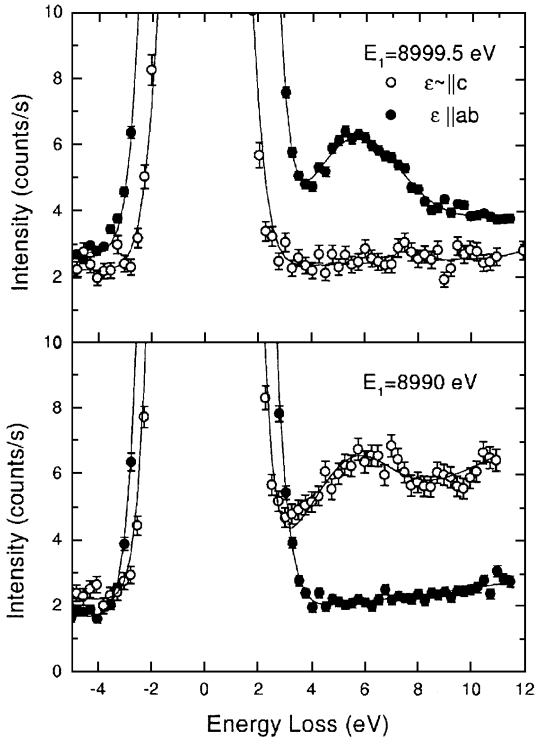

Fig. 6. Experimental polarization dependence of Cu $4p$-$1s$ RXES.[12] The open and closed circles correspond to the geometries (a) and (b), respectively. In the upper panel Ω is tuned at the absorption peak D, and in the lower panel Ω is tuned at B. The definition of D and B are given in Fig. 5.

(closed circles), and this fact certifies these peaks as a result of $1s$-$4p_\sigma$ transition. When $\boldsymbol{\epsilon} = \hat{x_1}$, the formula immediately gives the ratio of the absorption intensity as approximately

$$\sigma : \pi = \cos^2\theta_i : \sin^2\theta_i.$$

This result roughly explains the intensity ratio between the first and third features of the experimental XAS described in Fig. 5, where the ratio is found to be broadly consistent to $\sin^2 60^\circ : \cos^2 60^\circ = 3 : 1$ by considering a steeply increasing background spectrum. Now the first question has been answered.

The function $D^{\zeta}_{\hat{\beta}\hat{\alpha}}$ rules angular dependence of RXES. When $(\boldsymbol{\epsilon}', \boldsymbol{\epsilon}) = (\hat{y_2}, \hat{y_1})$, we see that there is no contribution of $4p_z$ ($4p_\pi$) orbitals because of $D^{z}_{\hat{y_2},\hat{y_1}} = 0$. This fact explains no enhancement over the $4p_\pi$ absorption threshold under the geometry (b). This is the answer to the second question. Next, we notice that $\hat{x_1} \to \hat{y_2}$ and $\hat{y_1} \to \hat{x_2}$ transitions are not allowed unless the ground state $|g\rangle$ is E representation of the D_{4h} group. If it is the case,

$$\langle f|T_x(\Omega)|g\rangle = \langle f|T_y(\Omega)|g\rangle$$

follows for a final state $|f\rangle$ with the same symmetry as $|g\rangle$ because $T_x = C_4 T_y (C_4)^3$, C_4 being the rotation operator of $\pi/4$ around the z-axis at a Cu site $\boldsymbol{R}$. Here we defined $T_\zeta(\Omega)$ by

$$T_\zeta(\Omega) = \sum_{\boldsymbol{R}} \mathrm{e}^{\mathrm{i}\boldsymbol{q}\cdot\boldsymbol{R}} S^\dagger_{\boldsymbol{R}} Q_{\zeta\boldsymbol{R}} G_0(\Omega) Q^\dagger_{\zeta\boldsymbol{R}} S_{\boldsymbol{R}}$$

for $\zeta = x, y$ and z, with $\boldsymbol{q} \perp \boldsymbol{R}$ in this case. Thus $D^{x}_{\hat{y_2}\hat{x_1}} = -D^{y}_{\hat{y_2}\hat{x_1}}$ or $D^{x}_{\hat{x_2}\hat{y_1}} = -D^{y}_{\hat{x_2}\hat{y_1}}$ leads to the zero transition amplitude. Note that one can not suppress the elastic line by choosing $\boldsymbol{\epsilon}\cdot\boldsymbol{\epsilon}' = 0$ as far as $\boldsymbol{q} \perp \boldsymbol{R}$ holds, because elastic as well as inelastic scattering is not allowed in this case.

Under the same assumption on the ground state, emission intensity under the geometry (b) is given as $I_2(\Omega) = |\langle f|T_x(\Omega)|g\rangle|^2$, and emission intensity under the geometry (a) as

$$I_1(\Omega) = |\langle f|T_x(\Omega)\cos(\theta_i+\theta)\cos\theta_i + T_z(\Omega)\sin(\theta_i+\theta)\sin\theta_i|g\rangle|^2 . \quad (3.1)$$

Thus we can estimate the intensity ratio between π- and σ-resonances under this geometry as

$$\sigma : \pi = \cos^2(\theta_i+\theta)\cos^2\theta_i : \sin^2(\theta_i+\theta)\sin^2\theta_i,$$

giving $\sigma : \pi = 1 : 9$ for $\theta_i = \theta = 60^\circ$. This ratio partly answers the third question, i.e. the little resonance enhancement when Ω passes by the $4p_\sigma$ threshold under the geometry (a), although the relatively large error bars prevent us from a further quantitative statement.

One can also roughly estimate the ratio of maximum intensity of the 5.7 eV peak for the two geometries. Since the maximum peak occurs at the $4p_\pi$ absorption threshold in the case of the geometry (a), we have $I_1 \sim \sin^2(\theta_i+\theta)\sin^2\theta_i |\langle f|T_z(\Omega_\mathrm{B})|g\rangle|^2$. If $|\langle f|T_z(\Omega_\mathrm{B})|g\rangle|$ can be regarded to be the same order as $|\langle f|T_x(\Omega_\mathrm{D})|g\rangle|$, the assumption that is exactly justified in the isotropic limit of $4p$ orbitals, we have the ratio as

$$I_1/I_2 \sim \sin^2(\theta_i+\theta)\sin^2\theta_i.$$

For $\theta_i = \theta = 60^\circ$, this is approximately 0.56, which broadly explains the ratio of the 5.7 eV intensity in Fig. 6 (the answer to the fourth question).

We have studied the Cu $4p$-$1s$ RXES under only the two geometries. Although the present calculation and experiment show no clear evidence that the assumption we put at the beginning of this subsection breaks down, it may be interesting to watch the angular and polarization dependence of RXES spectra in a class of materials. Ishihara and Maekawa have recently emphasized the role of anisotropy between $U_{4p3d}(\pi)$ and $U_{4p3d}(\sigma)$ to explain anomalous elastic scattering in orbital ordered Mn compounds.[22] Analyzing angular and polarization dependence of also inelastic scattering, it is expected to obtain more detailed information on the spatial direction of orbitals. This subject is left for the future study.

§4. Incident Energy Dependence

4.1 Calculated results

We carried out numerical calculations for the geometry (b) with the multi-Cu (Cu_5O_{16}) cluster and the single-Cu (Cu_1O_{256}) cluster models. Part of the results are shown in Fig. 5 with solid (multi-Cu) and dotted (single-Cu) curves for both panels. Corresponding to the experimental structures C and D in the XAS spectra, a doubly-peaked structure in the calculated absorption spectra is observed in the upper panel.[23] We hardly find discrepancy between the multi-Cu and single-Cu re-

sults, except for slight difference in the width of the main structure. The resonant behavior of the 5.7 eV peak shown in the lower panel is, however, quite different. The multi-Cu model presents a singly-peaked Ω-dependence, whereas the single-Cu model presents a doubly-peaked Ω-dependence. While the Ω-scan of the multi-Cu calculation reproduces much better than the single-Cu one, the experimental Ω-scan exhibits more definite suppression effect when Ω is tuned at the peak C.

To remove this discrepancy, we performed calculations including the reduction factor of the *d-p* transfer, R_c, which renormalizes the *d-p* transfer energy only around the photoexcited Cu site as $R_c \times T_{pd}$ in the intermediate state. Calculated XAS and RXES spectra with $R_c = 0.8$ are shown in Fig. 7. Despite the difference in the transition process, these figures are very similar to those of $4p_\pi$.[6] The only remarkable difference is that the main absorption structure is more broadened. This result is consistent to the experimental difference in line width between the peak A (B) and C (D).

The Ω-scan of the 5.7 eV peak based on these improved calculations is plotted in the lower panel of Fig. 8. We see that agreement with the experimental data (closed circles) is considerably improved in the multi-Cu result (solid curve). Specifically, the suppression effect when Ω is tuned at the main absorption peak is more clearly reproduced. While the inclusion of $R_c = 0.8$ also in the single-cluster case seems to give rise to more suppression as compared to that in Fig. 5, the overall line shape is still doubly-peaked, being utterly different from the experimental data.

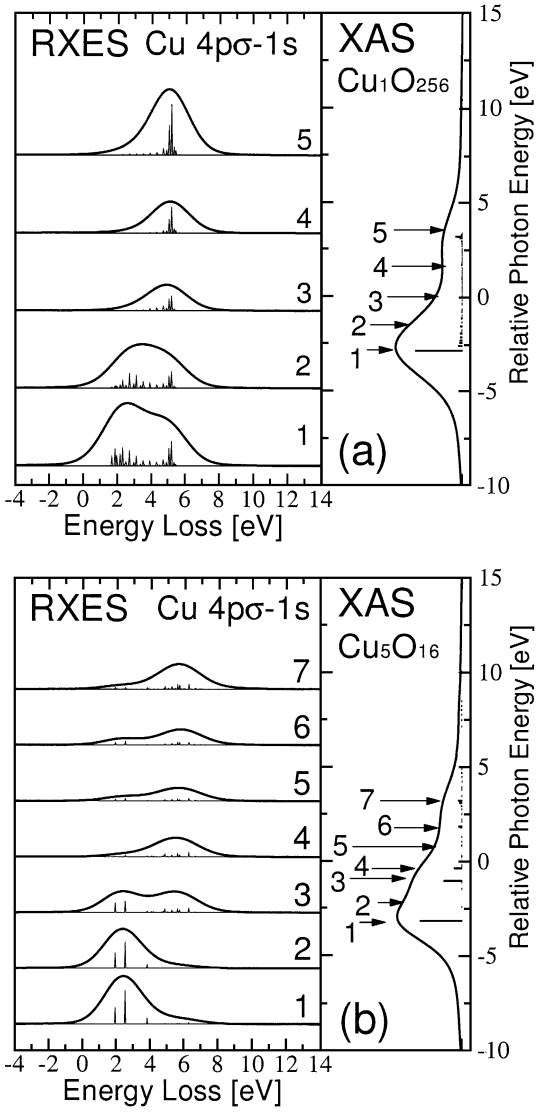

Fig. 7. Cu *K*-XAS and $4p_\sigma$-1*s* RXES with $R_c = 0.8$. (a) The impurity Anderson model (Cu_1O_{256} cluster). The XAS spectrum shown in the right panel is convoluted with Lorentzian $\Gamma_L = 0.8$ eV (HWHM) to consider lifetime of a 1*s* core hole, and further convoluted with Gaussian $\Gamma_G = 1.2$ eV (HWHM) to reproduce the experimental line width. The RXES spectrum shown in the left panel is also convoluted with $\Gamma_G = 1.15$ (HWHM) to reproduce the experimental resolution. (b) The multi-Cu model (Cu_5O_{16} cluster). The XAS spectrum shown in the right panel is convoluted with Lorentzian $\Gamma_L = 0.8$ eV (HWHM) to consider lifetime of a 1*s* core hole, and further convoluted with Gaussian $\Gamma_G = 0.8$ eV (HWHM) to reproduce the experimental line width. The RXES spectrum shown in the left panel is also convoluted with $\Gamma_G = 1.15$ (HWHM) to reproduce the experimental resolution. For (a) and (b), the elastic line, which should be located at zero, is omitted from the figure. The numbers attached to arrows in each XAS spectrum corresponds to those in RXES, representing the excitation energy.

4.2 Discussion

Because of the similarity between $4p_\pi$[6] and $4p_\sigma$, we naturally assign the main absorption peak calculated with the multi-Cu cluster to that state which has a Zhang-Rice (ZR) singlet at plaquettes neighboring to the photoexcited one. The shoulder (3 in Fig. 7(b)) of the

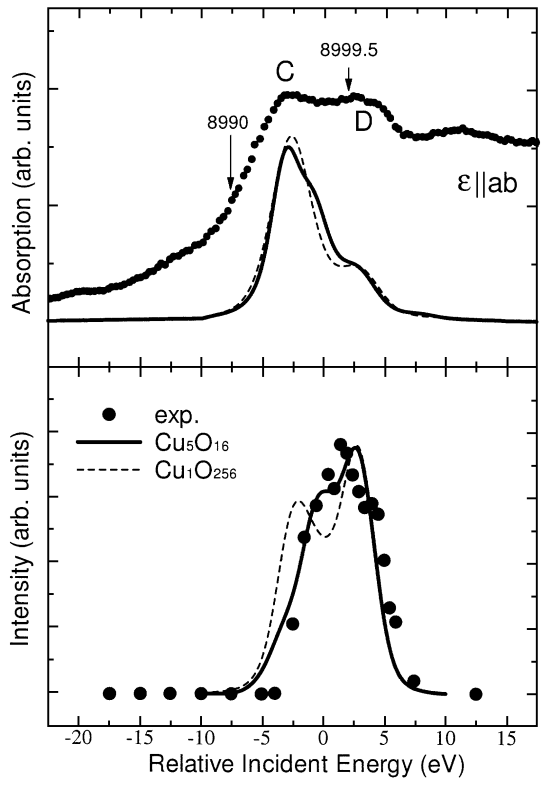

Fig. 8. The improved calculations of Cu *K*-XAS and the Ω-scan of the 5.7 eV inelastic peak with $R_c = 0.8$. The closed circles represent again the experimental results measured under the geometry (b) for both panels. See the caption in Fig. 5.

main structure is attributed to a well-screened $\underline{c}d^{10}\underline{L}$-like state, and the satellite peak (7 in Fig. 7(b)) is attributed to a poorly-screened $\underline{c}d^9$-like state, where $\underline{c}$ and $\underline{L}$ represent core and ligand holes, respectively. The main and satellite absorption peaks in the single-Cu model are, on the other hand, mainly $\underline{c}d^{10}\underline{L}$ and $\underline{c}d^9$ states, respectively.

Whichever model is used, there is a certain difference in spatial extent among these states, and this difference gives rise to the Ω-dependence of RXES spectra. As explained in the introduction, the ZR state has the most nonlocal character because a $3d$ hole is pushed out by the strong $1s$-$3d$ repulsive Coulomb interaction into neighboring plaquette, so that it has little overlap with intra-plaquette CT states (see Fig. 1). Although the $4p$-$3d$ correlation U_{4p3d} should more or less disturb the motion of the ZR singlet, it seems to act as only small perturbation. The final states are the same as those of $4p_\pi$-$1s$ RXES because of the absence of $4p$ electron. As discussed,[6] the 5.7 eV inelastic peak is a $d^{10}\underline{L}$-dominant anti-bonding state, and the 2 eV peak is attributed to an excitation of a $3d$ hole from the upper Hubbard band to the ZR singlet band. $R_c < 1$ affects spatial extent of the CT excitations in the intermediate state. In the ZR intermediate state, a $3d$ hole at the photoexcited Cu site should be pushed out more strongly to the neighboring plaquettes, so that the overlap with intra-plaquette CT state would get smaller. Consequently, $R_c < 1$ intensifies the suppression effect of the 5.7 eV peak.

§5. Momentum Transfer Dependence

The energy dispersion in a CuO_2 plane can be measured by sweeping the in-plane component of $\boldsymbol{q}$. In the context of local and nonlocal excitations, it is interesting to measure the energy dispersion over k-space, because an excited state completely localized in a unit cluster should exhibit no energy dispersion. We carried out numerical calculation on Cu $4p$-$1s$ RXES for a 1D periodic Cu_4O_{12} cluster for $q = 0$, $\pi/2$ and π in units of $(2a)^{-1}$. The results are shown in Fig. 9, where we adopt the same parameter set as that in Fig. 7(b) except for $U_{dc} = 8.0$.[24] Note that all core orbitals are taken into account here, whereas we have fixed a core hole to the central Cu site so far. Analogous to Fig. 7(b), the main absorption structure is composed of two peaks, and a satellite structure is observed about 7 eV distant from the main peak. Recent experimental and theoretical studies on high-resolution Cu $2p$-XPS of various cuprates show that the nonlocally screening path gives rise to the main peak of Cu $2p$-XPS in one-dimensional as well as two-dimensional cuprates, as far as the corner-shared structure is concerned.[25-28] Although close inspection shows that each spectrum has slight difference according to difference in physical parameters and dimensionality, the character of the shoulder of the main peak or the satellite structure is also broadly common to both dimensions.[29] Hence we can utilize the calculated results to infer $\boldsymbol{q}$-dependence of the CT excitations in Nd_2CuO_4.

For the q-dependence of the RXES spectra, we find in Fig. 9 that the 2 eV peak exhibits considerable q-dependence in its intensity and position. Recently, Abbamonte *et al.*[18] successfully observed q-dependence of the 2 eV peak, which was hidden in the tale of the elastic line in Fig. 6, in Cu $4p$-$1s$ RXES of a two-dimensional insulating cuprate, $Sr_2CuO_2Cl_2$. Moreover, their experimental data show that the CT structure at about 5 eV displays little q-dependence in its peak position.[30] This is qualitatively consistent to Fig. 9, and suggests the intra-plaquette nature of the 5.7 eV excitation in Nd_2CuO_4. On the contrary, the strong q-dependence of the 2 eV peak confirms the inter-plaquette (nonlocal) nature of the 2 eV CT excited state.

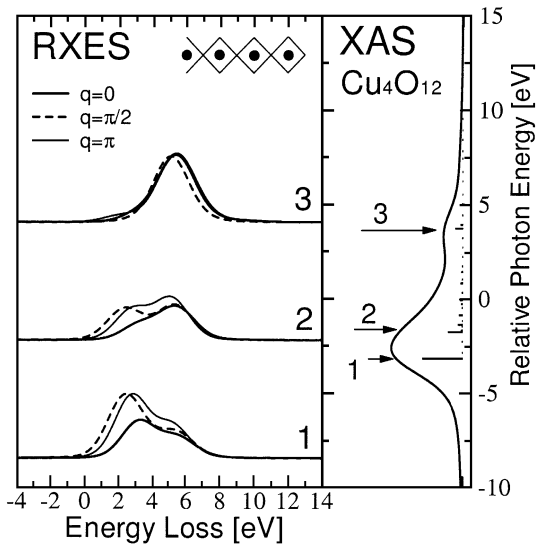

Fig. 9. The q-dependence of Cu $4p_\sigma$-$1s$ REXS for a one-dimensional cluster as shown in the inset. We see that the 2 eV CT excitation is strongly q-dependent, whereas the 5.7 eV peak has little q-dependence.

Note that a core hole is fixed to calculate RXES spectra in Fig. 7(b). Roughly speaking, this corresponds to that situation, where RXES spectra with all kinds of the momentum transfer $\boldsymbol{q}$ are mixed up. Figure 9 suggests that the 2 eV peak in Fig 7(b) might be excessively highlighted under this situation, as compared to the experimental data, where $\boldsymbol{q}$ is perpendicular to the CuO_2 plane. For detailed discussion, one needs experimental studies with higher resolution and theoretical studies with larger clusters.

§6. Conclusions

We have studied the polarization dependence of charge transfer excitations in Cu $4p$-$1s$ RXES of Nd_2CuO_4. We derived a closed expression on angular and polarization dependence of RXES. The experimental polarization dependence is successfully explained with the formula, and the fact that the incident polarization dependence of the excitation process may be exploited to select the intermediate state of the resonance is shown.

Next, we confirmed the mechanism of the suppression of resonant inelastic scattering for nonlocally screened intermediate states. The difference between $4p_\pi$ and $4p_\sigma$ gave no drastic change in XAS and RXES spectra. It was found that the agreement between the experiment and the calculation is considerably improved by taking

account of the configuration dependence of d-p transfer.

Finally, we examined the q-dependence of the CT excitations in RXES spectra. The calculated spectra showed, first, that the 5.7 eV peak displays little q-dependence, and second, that the 2 eV peak considerably depends on q. These are interpreted in terms of intra- and inter-plaquette natures of the excitations, and are regarded as further support of the explanation of the suppression effect.

Acknowledgements

The authors thank Dr. J. P. Hill, Dr. C.-C. Kao and Dr. K. Hämäläinen for sending their experimental data and fruitful discussions. This work is partly supported by a Grant-in-Aid for Scientific Research from the Ministry of Education, Science, Culture and Sports. The computation in this work was done using the facilities of the Super-Computer Center, Institute for Solid State Physics, The University of Tokyo.

1) M. Pompa, A. M. Flank, P. Lagarde, J. C. Rife, I. Stekhin, M. Nakazawa, H. Ogasawara and A. Kotani: Phys. Rev. B **56** (1997) 2267.
2) F. M. F. de Groot, M. Nakazawa, A. Kotani, M. H. Krish and F. Sette: Phys. Rev. B **56** (1997) 7285.
3) L. C. Duda, G. Dräger, S. Tanaka, A. Kotani, J. Guo, D. Heumann, S. Bocharov, N. Wassdahl and J. Nordgren: J. Phys. Soc. Jpn. **67** (1998) 416.
4) Pieter Kuiper, J.-H. Guo, Conny Såthe, L.-C. Duda, Joseph Nordgren, J. J. M. Pothuizen, F. M. F. de Groot and G. A. Sawatzky: Phys. Rev. Lett. **80** (1998) 5204.
5) Y. Harada, T. Kinugasa, R. Eguchi, M. Matsubara, A. Kotani, M. Watanabe, A. Yagishita and S. Shin: Phys. Rev. B **61** (2000) 12854.
6) T. Idé and A. Kotani: J. Phys. Soc. Jpn. **68** (1999) 3100.
7) Zhengquan Tan, J. I. Budnick, C. E. Bouldin, J. C. Woicik, S-W. Cheong, A. S. Cooper, G. P. Espinosa and Z. Fisk: Phys. Rev. B **42** (1990) 1037.
8) H. Oyanagi, Y. Yokoyama, H. Yamaguchi, Y. Kuwahara, T. Katayama and Y. Nishihara: Phys. Rev. B **42** (1990) 10136.
9) J. M. Tranquada, S. M. Heald, W. Kunnmann, A. R. Moodenbaugh, S. L. Qiu, Y. Xu, and P. K. Davies: Phys. Rev. B **44** (1991) 5176.
10) M. Matsubara, T. Uozumi, A. Kotani, Y. Harada and S. Shin: J. Phys. Soc. Jpn. **69** (2000) 1558.
11) J. P. Hill, C.-C. Kao, W. A. L. Caliebe, M. Matsubara, A. Kotani, J. L. Peng and R. L. Greene: Phys. Rev. Lett. **80** (1998) 4967.
12) K. Hämäläinen, J. P. Hill, S. Huotari, C.-C. Kao, L. E. Berman, A. Kotani, T. Idé, J. L. Peng and R. L. Greene: Phys. Rev. B **61** (2000) 1836.
13) M. A. van Veenendaal, H. Eskes and G. A. Sawatzky: Phys. Rev. B **47** (1993) 11462.
14) M. van Veenendaal and G. A. Sawatzky: Phys. Rev. B **49** (1994) 3473.
15) K. Okada and A. Kotani: Phys. Rev. B **52** (1995) 4794.
16) E. D. Isaacs, P. M. Platzman, P. Metcalf and J. M. Honig: Phys. Rev. Lett. **76** (1996) 4211.
17) P. M. Platzman and E. D. Isaacs: Phys. Rev. B **57** (1998) 11107.
18) P. Abbamonte, C. A. Burnes, D. D. Issacs, P. M. Platzman, L. L. Miller, S. W. Cheong and M. V. Klein: Phys. Rev. Lett. **83** (1999) 860.
19) K. Tsutsui, T. Tohyama and S. Maekawa: Phys. Rev. Lett. **83** (1999) 3705.
20) S. Matsuno and H. Kamimura: J. Superconductivity **7** (1994) 517.
21) R. D. Cowan: *The Theory of Atomic Structure and Spectra*, University of California Press, Berkeley, 1981.
22) S. Ishihara and S. Maekawa: Phys. Rev. B **58** (1998) 13442.
23) In the experimental spectra, there is strong contribution of the background, which would steeply increase from about 8980 eV.
24) This value of U_{dc} is taken in order to keep the main-satellite separation in XAS spectrum the same as that in Fig. 7(b).
25) K. Okada, A. Kotani, K. Maiti and D. D. Sarma: J. Phys. Soc. Jpn. **65** (1996) 1844.
26) K. Okada and A. Kotani: Physica B: Condens. Matter **237–238** (1997) 383.
27) T. Böske, K. Maiti, O. Knauff, K. Ruck, M. S. Golden, G. Krabbes, J. Fink, T. Osafune, N. Motoyama, H. Eisaki and S. Uchida: Phys. Rev. B **57** (1998) 138.
28) K. Karlsson, O. Gunnarsson and O. Jepsen: Phys. Rev. Lett. **82** (1999) 3528.
29) K. Okada and A. Kotani: J. Electron Spectrosc. Relat. Phenom. **86** (1997) 119.
30) They assign the 5 eV structure to a "shakeup" scattering. However, it has been established from our analysis[6] that this is the $d^{10}\underline{L}$-dominant anti-bonding state.